Observations of water with Herschel/HIFI toward the high-mass protostar AFGL 2591

Y. Choi, F. F. S. van der Tak, E. F. van Dishoeck, F. Herpin and F. Wyrowski

Context. Water is an important chemical species in the process of star formation, and a sensitive tracer of physical conditions in star-forming regions because of its rich line spectrum and large abundance variations between hot and cold regions.
Aims. We use spectrally resolved observations of rotational lines of H_2O and its isotopologs to constrain the physical conditions of the water emitting region toward the high-mass protostar AFGL 2591.
Methods. *Herschel*-HIFI spectra from 552 up to 1669 GHz show emission and absorption in 14 lines of H_2O, $H_2{}^{18}O$, and $H_2{}^{17}O$. We decompose the line profiles into contributions from the protostellar envelope, the bipolar outflow, and a foreground cloud. We use analytical estimates and rotation diagrams to estimate excitation temperatures and column densities of H_2O in these components. Furthermore, we use the non-LTE radiative transfer code RADEX to estimate the temperature and volume density of the H_2O emitting gas.
Results. Assuming LTE, we estimate an excitation temperature of ~42 K and a column density of $\sim 2\times 10^{14}$ cm^{-2} for the envelope and ~45 K and 4×10^{13} cm^{-2} for the outflow, in beams of 4″ and 30″, respectively. Non-LTE models indicate a kinetic temperature of ~60–230 K and a volume density of $7\times10^{6}-10^{8}$ cm^{-3} for the envelope, and a kinetic temperature of ~70–90 K and a gas density of $\sim10^{7}-10^{8}$ cm^{-3} for the outflow. The ortho/para ratio of the narrow cold foreground absorption is lower than three (~1.9±0.4), suggesting a low temperature. In contrast, the ortho/para ratio seen in absorption by the outflow is about 3.5±1.0, as expected for warm gas.
Conclusions. The water abundance in the outer envelope of AFGL 2591 is $\sim10^{-9}$ for a source size of 4″, similar to the low values found for other high-mass and low-mass protostars, suggesting that this abundance is constant during the embedded phase of high-mass star formation. The water abundance in the outflow is $\sim10^{-10}$ for a source size of 30″, which is ~10× lower than in the envelope and in the outflows of high-mass and low-mass protostars. Since beam size effects can only increase this estimate by a factor of 2, we suggest that the water in the AFGL 2591 outflow is affected by dissociating UV radiation due to the low extinction in the outflow lobe.

Astrochemistry at work in the L1157–B1 shock: acetaldehyde formation

C. Codella, F. Fontani, C. Ceccarelli, L. Podio, S. Viti, R. Bachiller, M. Benedettini and B.Lefloch

ABSTRACT

The formation of complex organic molecules (COMs) in protostellar environments is a hotly debated topic. In particular, the relative importance of the gas phase processes as compared to a direct formation of COMs on the dust grain surfaces is so far unknown. We report here the first high-resolution images of acetaldehyde (CH_3CHO) emission towards the chemically rich protostellar shock L1157-B1, obtained at 2 mm with the IRAM Plateau de Bure interferometer. Six blueshifted CH_3CHO lines with E_u = 26-35 K have been detected. The acetaldehyde spatial distribution follows the young ($\sim$ 2000 yr) outflow cavity produced by the impact of the jet with the ambient medium, indicating that this COM is closely associated with the region enriched by iced species evaporated from dust mantles and released into the gas phase. A high CH_3CHO relative abundance, 2–3 $\times$ 10^{-8}, is inferred, similarly to what found in hot-corinos. Astrochemical modelling indicates that gas phase reactions can produce the observed quantity of acetaldehyde only if a large fraction of carbon, of the order of 0.1%, is locked into iced hydrocarbons.

1. CH3+HCOラジカル反応　T>30K のダスト上
2. CH4,CO2、。。の氷へ光励起
3. 氷マントルの昇華→高密度の気相で反応

動的時間　2000年
衝撃波領域と考えられる

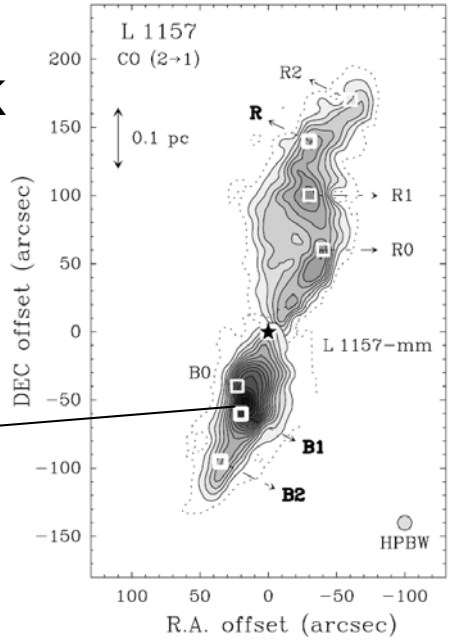

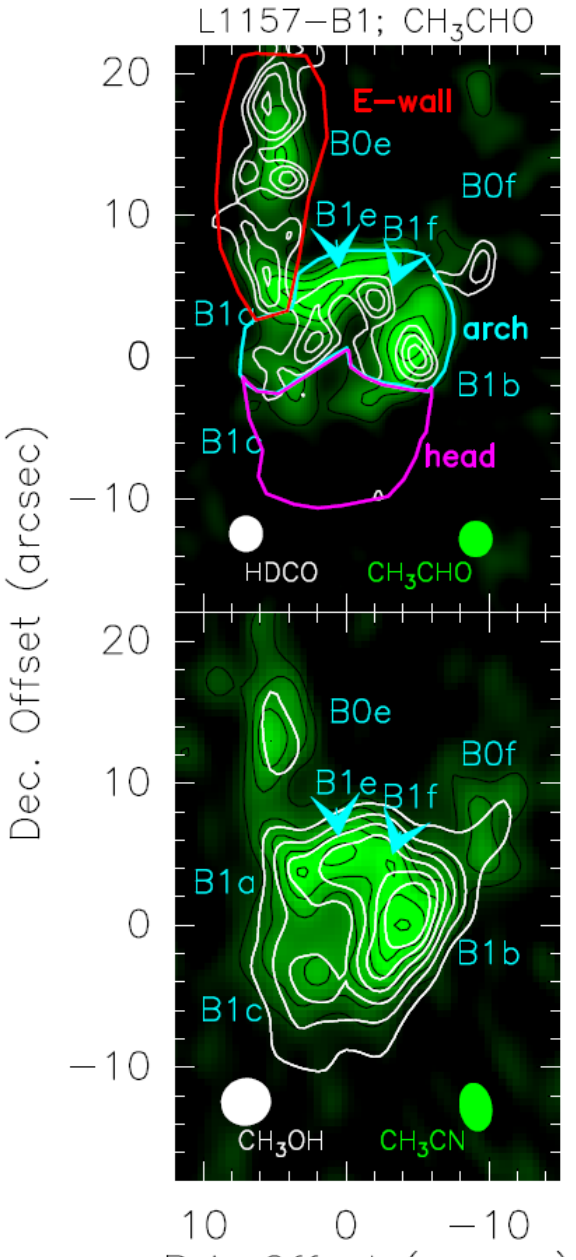

アセトアルデヒドの量
２－3x10^－８

原料の炭化水素C2H5量
2-6x10^-7

⇕

L1527-mm protostar近辺
X(CH4)~0.4–1.5× 10−5
← CH3Dの観測（Sakai12）から

a large fraction of carbon, of the order of 0.1%, is locked into iced hydrocarbons.

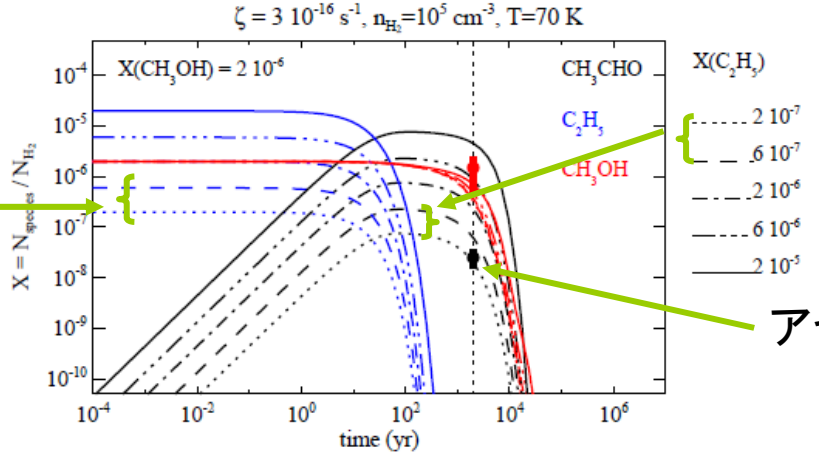

アセトアルデヒド

Figure 3. Evolution of acetaldehyde (CH_3CHO, black), (C_2H_5, blue), and methanol (CH_3OH, red) abundances in the shock as a function of time. Observed abundances (colour circles) are over-plotted at the shock age ($t_{shock} \sim 2000$ years, vertical dotted line). The evolution is computed from steady-state values in the cloud ($n_{H_2} = 10^4$ cm^{-3}, $T_{kin} = 10$ K, $\zeta = 3 \times 10^{-16}$ s^{-1}) by enhancing the gas temperature and density ($n_{H_2} = 10^5$ cm^{-3}, $T_{kin} = 70$ K), and the abundance of molecules which are thought to be sputtered off dust grain mantles. We set $X_{CO_2} = 6 \times 10^{-5}$ and $X_{OCS} = 6 \times 10^{-6}$ as in Podio et al. 2014, $X_{CH_3OH} = 2 \times 10^{-6}$ (Mendoza et al. 2014), and vary the abundance of C_2H_5 between 2×10^{-7} and 2×10^{-5}.

The Interstellar Medium and star formation on kpc size scales Clare L. Dobbs

ABSTRACT

By resimulating a region of a global disc simulation at higher resolution, we resolve and study the properties of molecular clouds with a range of masses from a few 100's $M_\odot$ to 10^6 $M_\odot$. The purpose of our paper is twofold, i) to compare the ISM and GMCs at much higher resolution compared to previous global simulations, and ii) to investigate smaller clouds and characteristics such as the internal properties of GMCs which cannot be resolved in galactic simulations. We confirm the robustness of cloud properties seen in previous galactic simulations, and that these properties extend to lower mass clouds, though we caution that velocity dispersions may not be measured correctly in poorly resolved clouds. We find that the properties of the clouds and ISM are only weakly dependent on the details of local stellar feedback, although stellar feedback is important to produce realistic star formation rates and agreement with the Schmidt-Kennicutt relation. We study internal properties of GMCs resolved by $10^4 - 10^5$ particles. The clouds are highly structured, but we find clouds have a velocity dispersion radius relationship which overall agrees with the Larson relation. The GMCs show evidence of multiple episodes of star formation, with holes corresponding to previous feedback events and dense regions likely to imminently form stars. Our simulations show clearly long filaments, which are seen predominantly in the inter-arm regions, and shells.

Global simulation（Dobbs & Pringle 2013）
から1kpc^2領域を切り出して、時間を巻き戻し、
粒子数を増やして再計算
質量分解能300→3.8Msol

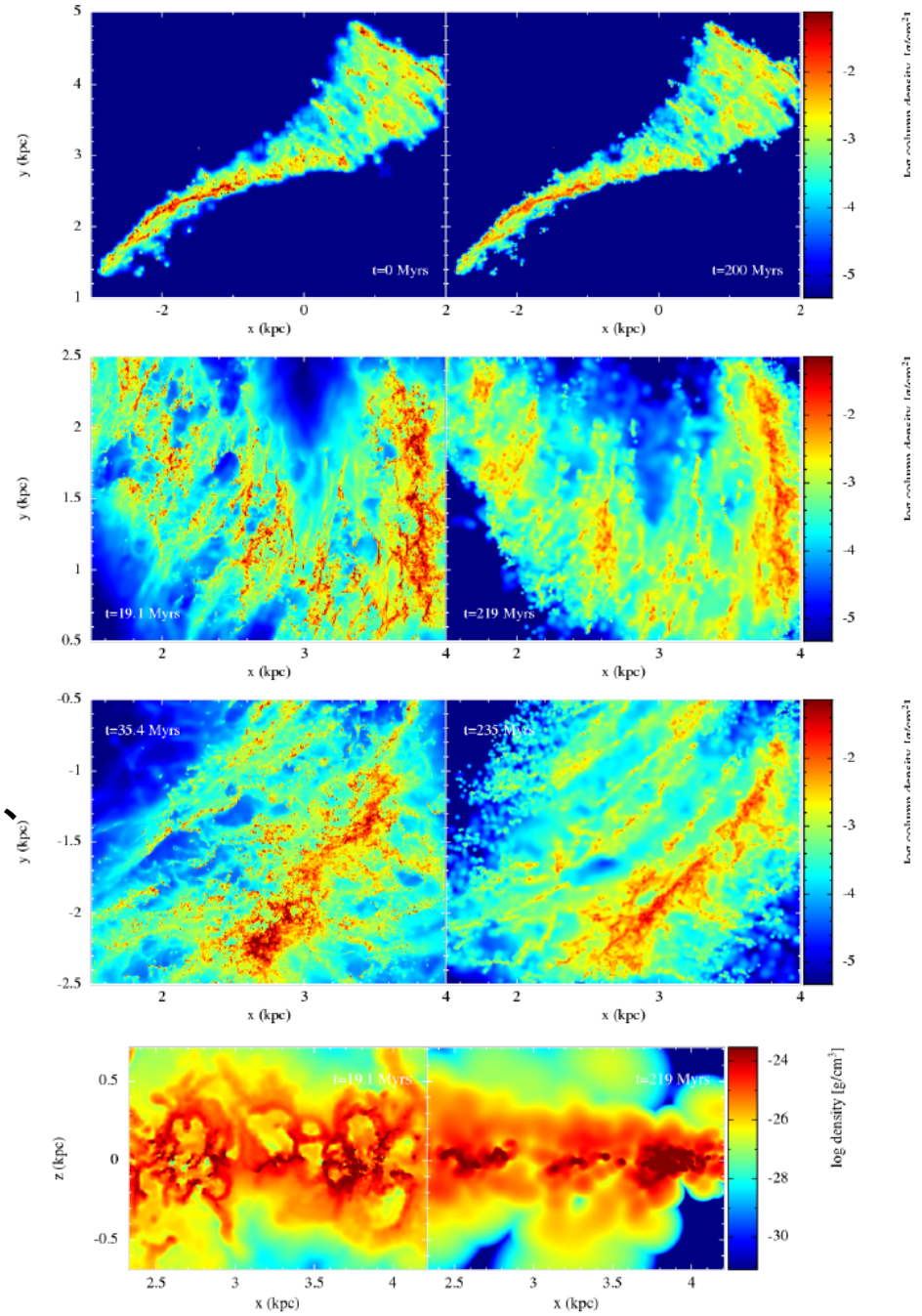

resimulation　　Original global simulation

再計算　　オリジナル

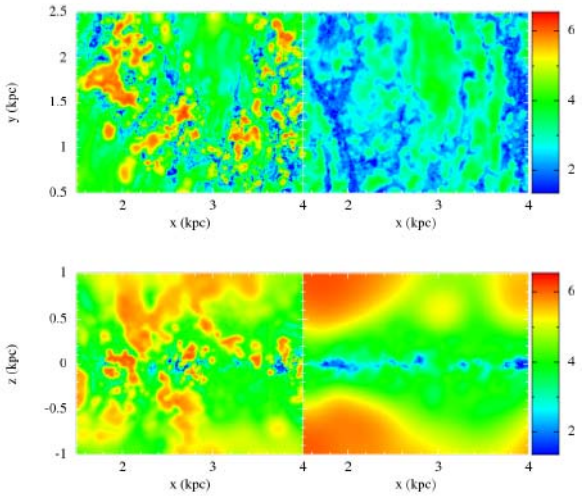

Figure 2. Comparison of the temperature in the resimulation (left) and original global calculation (right), at a time of 19 Myr in the resimulation. All panels show cross sections, the top panels show cross sections in the xy plane, the lower panels show cross sections in the xz plane. Hot gas is clearly more prominent in the resimulation compared to the global simulation, and much finer structure can again be seen in the resimulation.

円盤中の高温ガスの構造が違う

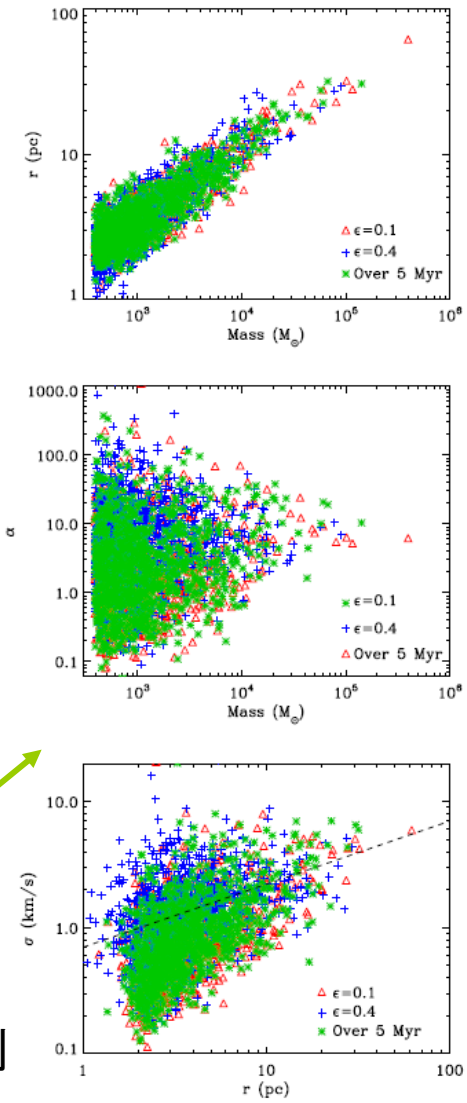

Figure 7. Cloud properties are compared for different feedback prescriptions (all for the high resolution resimulation). The panels show mass and radius (top), virial parameter (middle) and velocity dispersion (lower panel). The dashed line on the lower panel shows $\sigma = 0.7(r/1\mathrm{pc})^{0.5}$ km s^{-1}.

Larson則

星形成
P cr=500cm^-3
∇・v<0

$$E = \frac{\epsilon \times M(H_2) \times 10^{51}}{160 M_\odot} ergs$$

Efficiency 0.1,0.4
瞬間的、2～5Myr間

KS則

この計算

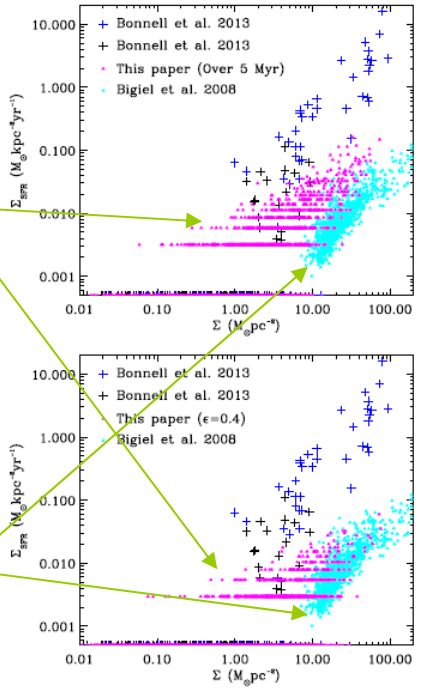

Bigiel+08　subkpc スケールの
KS則

Synthetic CO, H2 and Hi surveys of the Galactic 2nd Quadrant, and the properties of molecular gas

A. Duarte-Cabral, D. M. Acreman, C. L. Dobbs, J. C. Mottram, S. J. Gibson, C. M. Brunt, and K. A. Douglas

We present CO, H_2, HI and HISA distributions from a set of simulations of grand design spirals including stellar feedback, self gravity, heating and cooling. We replicate the emission of the 2nd Galactic Quadrant by placing the observer inside the modelled galaxies and post process the simulations using a radiative transfer code, so as to create synthetic observations. We compare the synthetic datacubes to observations of the 2nd Quadrant of the Milky Way to test the ability of the current models to reproduce the basic chemistry of the Galactic ISM, as well as to test how sensitive such galaxy models are to different recipes of chemistry and/or feedback.

We find that models which include feedback and self-gravity can reproduce the production of CO with respect to H_2 as observed in our Galaxy, as well as the distribution of the material perpendicular to the Galactic plane. While changes in the chemistry/feedback recipes do not have a huge impact on the statistical properties of the chemistry in the simulated galaxies, we find that the inclusion of both feedback and self-gravity are crucial ingredients, as our test without feedback failed to reproduce all of the observables. Finally, even though the transition from H_2 to CO seems to be robust, we find that all models seem to underproduce molecular gas, and have a lower molecular to atomic gas fraction than is observed. Nevertheless, our fiducial model with feedback and self-gravity has shown to be robust in reproducing the statistical properties of the basic molecular gas components of the ISM in our Galaxy.

Table 2. Statistical properties from the observations and the four galactic simulations.

Name	X_{CO} [10^{20} cm^{-2} K^{-1} km^{-1} s]	α (from $M \propto S^{\alpha}$)	$M(H_2)^{CO}$ [10^5 M$_\odot$]	$M(H_2)^{SPH(a)}$ [10^5 M$_\odot$]	Fraction$^{(b)}$	H/H$_2$$^{(a)}$
Observations	$2.0\,(\pm 0.9)$	1.1 ± 0.1	33	-	$20-80\%^{(c)}$	$\sim 6^{(d)}$
Fiducial	$2.5\,(\pm 0.9)$	1.8 ± 0.6	5	10	$\sim 50\%$	85
Strong Self Shielding	$1.9\,(\pm 0.9)$	2.4 ± 0.5	5	13	$\sim 40\%$	80
High Surface Density	$1.9\,(\pm 0.8)$	2.2 ± 0.3	139	60	$\sim 100\%^{(e)}$	29
No Feedback	$4.5\,(\pm 1.9)$	1.6 ± 0.3	74	235	$\sim 30\%$	6

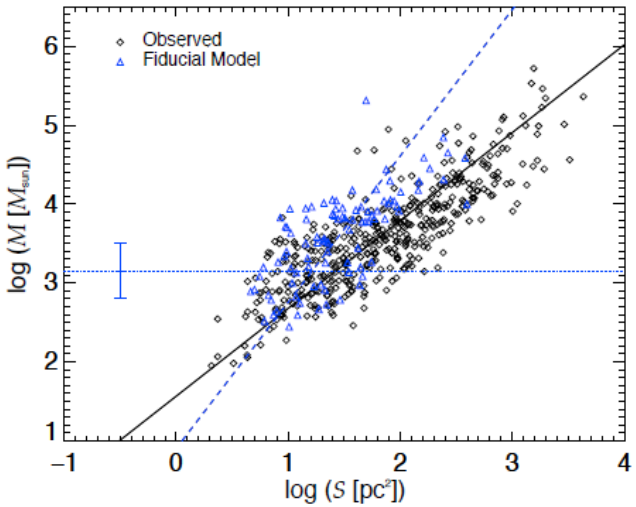

Larson則　M∝S^α

観測 α~1.1、計算 α~1.8

Figure 8. Comparison of the cloud masses versus the cloud (projected) sizes as extracted from the CO emission, for the observations (in black diamonds) and for the fiducial galaxy model (in blue triangles). The respective linear fits to the log-log space, corresponding to $M \propto S^{\alpha}$ are shown in black solid and blue dashed lines. Observations retrieve $\alpha = 1.1 \pm 0.1$ while the fiducial model has a steeper slope, with $\alpha = 1.8 \pm 0.6$. The blue dotted horizontal line indicates the average masses that we expect to be resolved, with an estimated level of the uncertainty shown with the error bar.

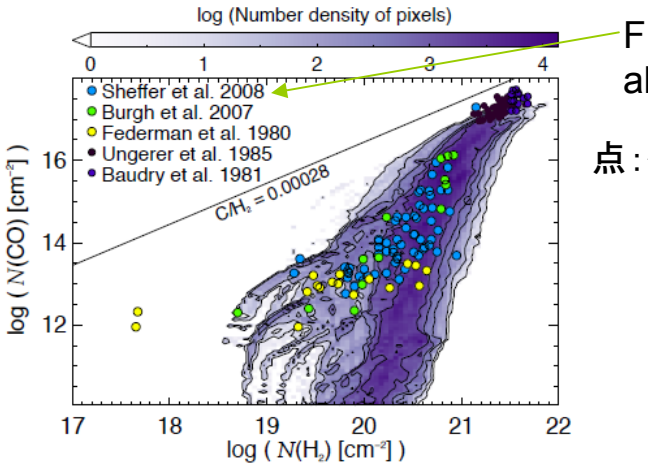

FUSE H2 absorption

点：観測、カラーは計算

Figure 4. Distribution of the CO column density against the H_2 column density from Galactic observations in the literature (coloured circles) and from the fiducial galaxy model (contours and colour scale). As in Sheffer et al. (2008), the line with $C/H_2 = 2.8 \times 10^{-4}$ shows the observational limit for the formation of CO based on the supply of atomic carbon (i.e. the abundance of C/H) from Cardelli et al. (1996).

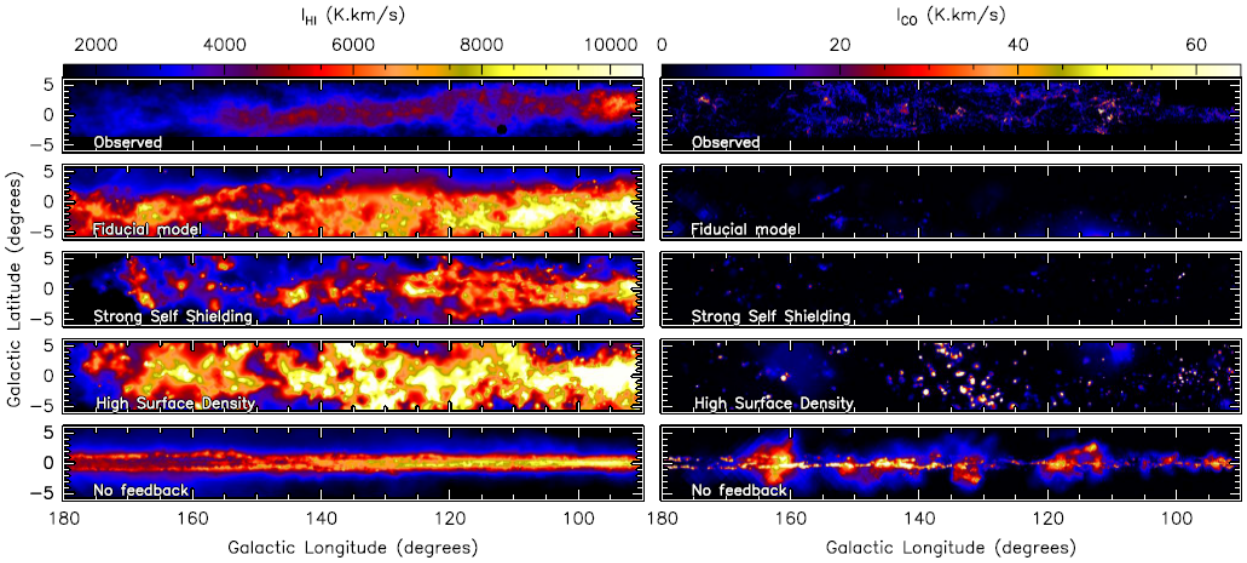

Figure 10. Comparison of the observed l-b distribution of HI (*left column*) and CO (*right column*) integrated intensity from the second quadrant of the Galaxy (top row) and the galactic models (on rows below).

The Gould Belt Very Large Array Survey IV: The Taurus-Auriga complex

Sergio A. Dzib, Laurent Loinard, Luis F. Rodrguez, Amy J. Mioduszewski, Gisela N. Ortiz-Leon, Marina A. Kounkel, Gerardo Pech, Juana L. Rivera, Rosa M. Torres, Andrew F. Boden, Lee Hartmann, Neal J. Evans II, Cesar Brice and John Tobin

We present a multi-epoch radio study of the Taurus-Auriga star-forming complex made with the Karl G. Jansky Very Large Array at frequencies of 4.5 GHz and 7.5 GHz. We detect a total of 610 sources, 59 of which are related to young stellar objects and 18 to field stars. The properties of 56% of the young stars are compatible with non-thermal radio emission. We also show that the radio emission of more evolved young stellar objects tends to be more non-thermal in origin and, in general, that their radio properties are compatible with those found in other star forming regions. By comparing our results with previously reported X-ray observations, we notice that young stellar objects in Taurus-Auriga follow a Güdel-Benz relation with κ=0.03, as we previously suggested for other regions of star formation. In general, young stellar objects in Taurus-Auriga and in all the previous studied regions seem to follow this relation with a dispersion of $\sim$ 1 dex. Finally, we propose that most of the remaining sources are related with extragalactic objects but provide a list of 46 unidentified radio sources whose radio properties are compatible with a YSO nature.

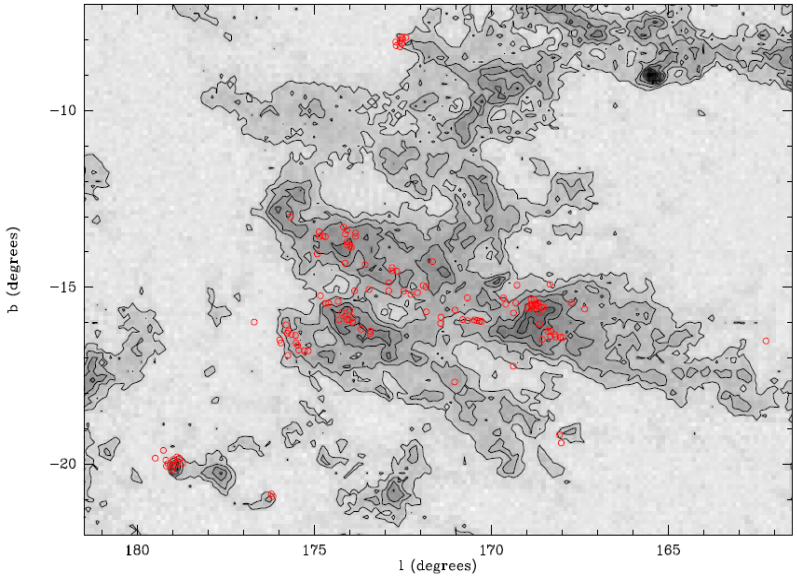

Fig. 6.— X-ray luminosity as a function of radio luminosity. The red line corresponds to the Güdel-Benz relation with $\kappa = 1$. The blue line correspond to the Güdel-Benz relation but with $\kappa = 0.03$. Symbols indicate the evolutionary status of the object as explained at the top-left of the diagram. Colors indicates YSOs in different star forming regions: Taurus (blue, this work), Ophiuchus (green, Dzib et al. 2013a), Serpens-W40 (red, Ortiz-León et al. 2014, submitted) and Orion (yellow, Kounkel et al. 2014). Open symbols indicate sources whose radio emission is thermal and solid symbols indicates non-thermal radio sources.

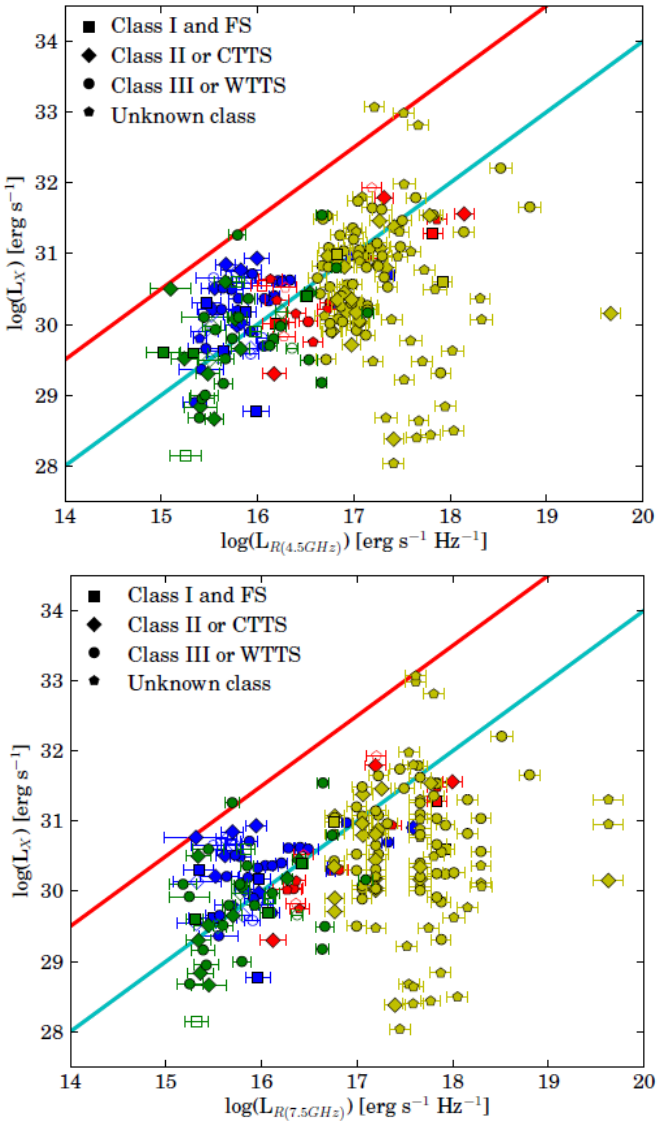

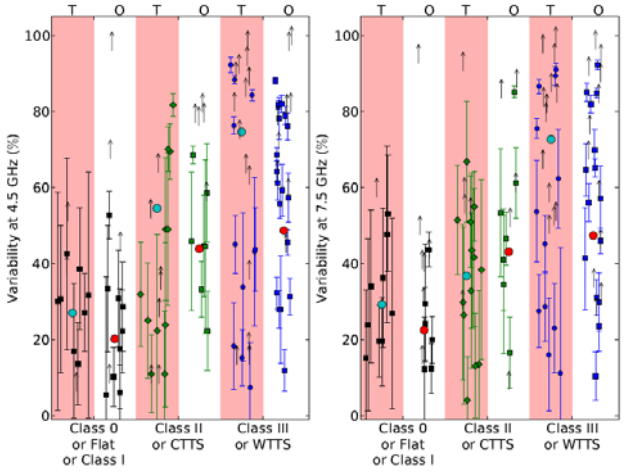

Fig. 3.— Variability at 4.5 GHz (left) and 7.5 GHz (right) as a function of YSO evolutionary status. We have labeled in the top with a T and an O if the sources are in Taurus or Ophiuchus, respectively. The individual sources are shown with their error bars, and the turquoise and red circles indicate the mean variability for each category in Taurus-Auriga and Ophiuchus, respectively. Ophiuchus data from Dzib et al. (2013a).

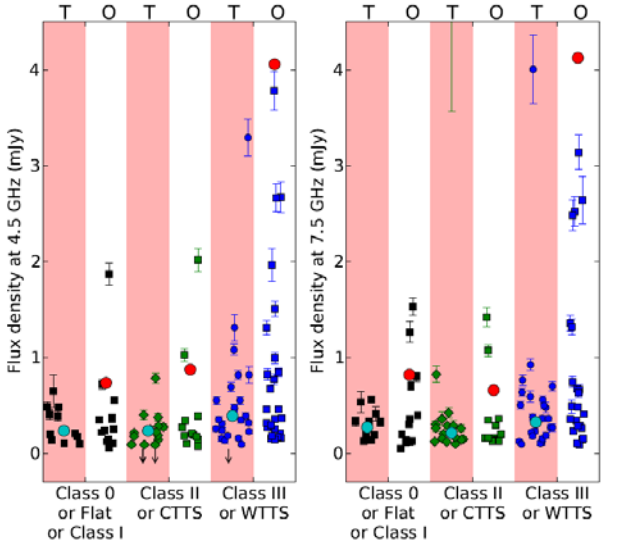

Fig. 4.— Radio flux at 4.5 GHz (left) and 7.5 GHz (right) as a function of YSO evolutionary status. We have labeled in the top with a T and an O if the sources are in Taurus or Ophiuchus, respectively. As in the previous figures, the individual sources are shown with their error bars, and the turquoise and red circles indicate the mean flux for each category in Taurus-Auriga and Ophiuchus, respectively. Ophiuchus data from Dzib et al. (2013a). We limit the figure to a flux of 4.5 mJy to see the slope between the mean fluxes in Taurus.